ISSN 1392-1320 MATERIALS SCIENCE (MEDŽIAGOTYRA). Vol. XX, No. X. 2026

Experimental and Numerical Investigation of Thinning Behavior in Deep Drawing of AISI 1008, CuZn30, and Aluminum 1100

Riham Raad AHMED [1], İsmail Hakkı KARA [1]*, Muhsin J. JWEEG [2]

[1] *Metallurgy and Materials Engineering Department of Engineering Faculty, Karabük University, Karabük,78050, Turkey*
[2] *College of Technical Engineering, Al-Farahidi University, Baghdad, Iraq*

http://doi.org/10.5755/j02.ms.43434

Received 27 October 2025; accepted 29 January 2026

This study investigates the thickness distribution behavior of deep drawing cup products under the influence of various forming parameters, die radius, punch velocity, blank holder force, sheet thickness, and sheet metal type. Three types of sheet metal were used: low carbon steel (AISI 1008), aluminum (1100), and brass (CuZn30), in sheets of 80 mm diameter circular blanks with thicknesses of 0.7 and 1 mm, formed by a tooling set (die, punch, and blank holder). The die radius profile at R4 and R6 was used, where the punch velocities were 100, 150, and 200 mm/min. ABAQUS/CAE was used for numerical simulation, and a dynamic explicit solver was employed to form cylindrical cup products. The results show that for three metals, higher punch speeds tend to increase strain localization, and maximum thinning occurs at the punch nose radius; the maximum thickening in the sidewall region and thinning are increased with the decrease of die radius. It was also found that the r-value of the Lankford coefficients plays a significant role in thinning behavior in relation to rolling (r-value direction). The results also indicate that aluminum alloys are relatively formable, but they are highly sensitive to process variables, specifically blank holder pressure and sheet thickness. Wrinkles are reduced by increased blank holder force, but higher values cause tearing near the punch corners. All of the materials showed a similar thinning behavior during the deep drawing process, in spite of the variations in their mechanical properties. The results have shown a strong agreement between experimental and numerical work with a maximum discrepancy of 5 %.
Keywords: deep drawing, thining, blank holder force, FES.

1. INTRODUCTION

Deep drawing is one of the most widely used production methods. Components of various shapes, including those with simple or complicated geometries, can be created using this technique [1]. In the sheet metal forming process, many factors have to be considered, such as blank holder force, drawing force, friction force, etc. The energy source for this deformation may be a mechanical press, a hydraulic press, or a high-explosive charge at the other [2]. The blank is clamped between the blank holder and the die during the deep drawing process. The blank holder is loaded by a blank holder force, which is required to control the material flow into the die cavity and prevent wrinkling. The circular blank was forced into the space between the die and the punch using the tooling set's punch, and as a result, the blank was fabricated into cylindrical, conical, or box-shaped products [3]. The three most common defect types apparent in the deep drawing are fracture, wrinkling, and thinning; these defects connect to product safety and performance [4]. Low carbon steel is commonly used in forming because of its strength and strain hardening, which improve resistance to deformation [5, 6]. Aluminum is low density and resistant to corrosion, its strength and hardening capacity are limited, which causes failure earlier [7, 8]. Brass (CuZn30), which has a higher density than aluminum and a lower strength than steel, provides a satisfactory balance between ductility and strength [9, 10].

In a different study. Sherbiny et al. [11] showed how a die and punch radius affects residual stresses and thickness distribution during deep drawing operations. Bouchaâla et al. [12] Larger die and punch radii allow the material flow more efficiently and reduce strain concentration when deep drawing process. Zein et al. [13] focused on the fact that using a finite element simulation to assess thickness distribution in deep drawing can greatly reduce production costs, time, and material loss. Tomáš et al [14] found that anisotropic material behavior is essential for achieving accurate predictions of thickness variation in the drawn part. Mousa et al. [15] looked at how thickness changes in different directions using ABAQUS finite element modeling, focusing on three important factors: die radius, friction coefficient, and blank holder force. Choubey et al. [16] study effect of anisotropy and strain rate on AISI 304 stainless steel flow characteristics when using a conical die. They conducted finite element simulations and examined these factors using the Ansys software. The results, the strain varied more in the $r0$ and $r45$ directions than in the $r90$ direction. Additionally, earing took place in the $r45$ direction, according to the planar isotropy values. Chen et al [17] study the varying blank holder force distributions to reduce earing and achieve more uniform thickness in aluminum AA1100 deep drawing, confirming the strong influence of BHF on thickness variation.

In this work, the effects of die radius, punch velocity, sheet thickness, and sheet metal type on the thickness variation in deep drawing cups made from low carbon steel

* Corresponding author: I.H. Kara
E-mail: *ihakkikara@karabuk.edu.tr*

AISI1008, aluminum AA1100 and brass CuZn30 are investigated. It is important to make these interactions for optimizing industrial forming processes, make products quality, and prevent it from failure. The finite element method will be used in both experiments and numerical methods.

2. NUMERICAL SIMULATION

A finite element analysis was conducted using ABAQUS version 23 to simulate the deep drawing process for cylindrical cup products made from low carbon steel AISI 1008, aluminum AA1100, and brass CuZn30, with sheets of thicknesses 0.7 mm and 1 mm, and an 80 mm circular blank. The four main parts of the finite element model used during this study are the die, punch, blank, and blank holder. Fig. 1 illustrates the geometry constructed in the ABAQUS/CAE pre-processor. For the rigid parts (die, punch, and blank holder), meshing was performed using R3D4 and R3D3 elements, which are specifically designed for rigid body definitions, with a global mesh size of 1.5 mm. For the deformable part (blank), use C3D8R and C3D6 elements, which correspond to 8-node and 6-node 3D elements with lower integration. A surface-to-surface dynamic explicit method was used for effective contact modeling of the interaction between rigid and deformable parts, utilizing a finite "sliding penalty" based contact algorithm associated with three contact pairs: die-bottom blank, punch-top blank, and holder-top blank. The simulation loading sequence was carried out in three steps. The process began with the initial step, during which the boundary conditions were applied. The second step represents the application of the blank holding force to secure the sheet in place.

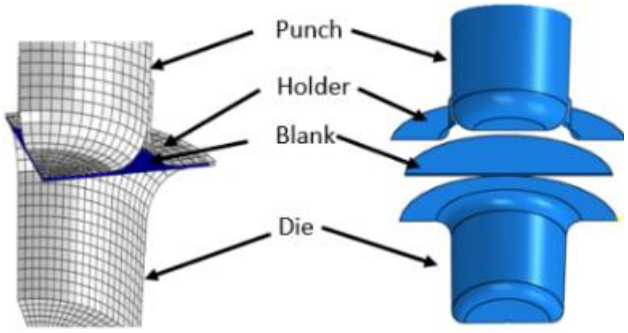

Fig. 1. Assembled model and meshing using ABAQUS

Fig. 2 shows the steps to make the circular metal cup in the ABAQUS program.

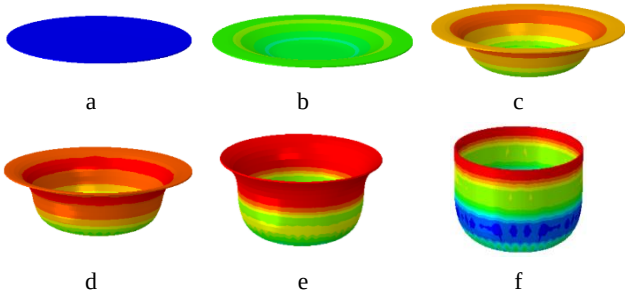

Fig. 2. Analysis of a cylindrical cup

3. EXPERIMENTAL DETAILS

3.1. Materials and mechanical properties

The chemical compositions of these materials are tested using an atomic absorption spectrometer based on the ASTM E 415-14 standard and the results are detailed in Table 1, Table 2, and Table 3.

Table 1. The chemical composition of the low carbon steel

C	Mn	Ni	Mo	Si	Cr	S	Al	Fe
0.07	0.03	0.027	0.003	0.08	0.03	0.02	0.048	Bal

Table 2. The chemical composition of Aluminum 1100

Fe	Mn	Si	Sn	Ti	Cr	Zn	Cu	Al
0.13	0.003	0.03	0.3	0.012	0.023	0.016	0.05	Bal

Table 3. The chemical composition of Brass CuZn30

Cu	Zn	P	Cr	Ni	Sn	Pb	Fe
68.5	31.09	0.019	0.004	0.0024	0.002	0.0065	0.056

To characterize the mechanical properties of the materials, tensile specimen rods were machined from sheet specimens in accordance with ASTM E8M standards using a water jet machine. As seen in Fig. 3 the specimens were prepared in three directions with respect to the rolling direction: 0°(rolling), 45°(diagonal), and 90°(transverse) [14, 18]. Fig. 4 shows the relationship between true stress-strain of the three materials. The r-values for the three rolling directions were calculated using Eq. 1 and Eq. 2 [2, 19]. The normal anisotropy ($\bar{r}$) and planar anisotropy (Δr),) values are shown in Table 4.

$$\bar{r} = \frac{1}{4}(r_0 + 2r_{45} + r_{90}); \quad (1)$$

$$\Delta r = \frac{1}{2}(r_0 - 2r_{45} + r_{90}). \quad (2)$$

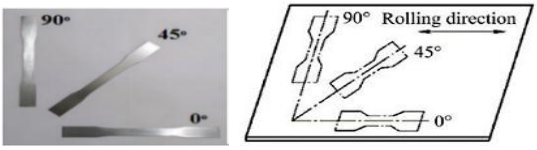

Fig. 3. Tensile specimen orientation for specifying (r) and (Δr)

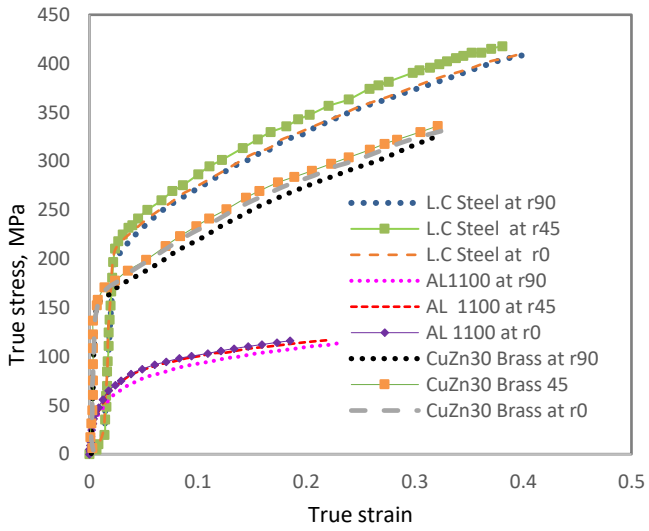

Fig. 4. The relationship between true stress- true strain curves along with different angles to the rolling direction

According to the experiments, Table 4 summarizes the mechanical properties that were obtained through experimentation.

Table 4. Mechanical properties of materials at different angles with respect to the rolling direction

Materials	Rolling direction	Yield stress, MPa	Tensile strength, MPa	r	$\bar{r}$	Δr
L.C steel AISI1008	0°	206	375	1.23	1.31	0.48
	45°	212	381	1.07		
	90°	216	408	1.89		
AA1100	0°	101	121	0.92	0.74	0.61
	45°	108	125	0.44		
	90°	112	130	1.17		
Br CuZn30	0°	161	317	1.28	1.85	0.30
	45°	155	331	1.03		
	90°	158	340	1.4		

The maximum r-value for low-carbon steel AISI 1008 was found at 90°, and the minimum value was found at 45°. This is in line with what other studies have found about low-carbon steels [19]. Aluminum AA1100, show the range of *r*-values from 0.44 to 1.17 when is closely near to the previous study which they found range from 0.45 to 1.18 [8]. This property can be taken To know concerning the way a material's anisotropy works.

3.2. Tooling and equipment

Metals with three different speed variables of punch (100, 150, and 200 mm/min) were used to draw circular blanks of 80 mm at the thickness of 0.7 mm and 1 mm. To account for the thickness of the sheet, the die profile radius of 4 mm and 6 mm with a punch radius of 4 mm are made of tool steel and machined by CNC turning and wire cutting. The punches and dies used in this study are shown in Fig. 5 and the drawing set arrangement is shown in Fig. 6. Blank holder force (BHF) can be determined by [2, 19]:

$$\text{BHF} = (\pi/4)\,[D_b - (d_1 + 2r)^2]\,P_d, \quad (3)$$

where P_d is the blank holder pressure (MPa), it can be found from:

$$Pd = (0.2\sim0.3)\,[(\beta - 1)^3 + D_p/200\,t]\,\sigma_u, \quad (4)$$

where t is material thickness (mm); D_b is the diameter of the blank (mm); D_p is the diameter of the punch; β is the draw ratio D_b/D_p.

Generally, Blank Holder Force (BHF) is approximately one-third of the drawing force.

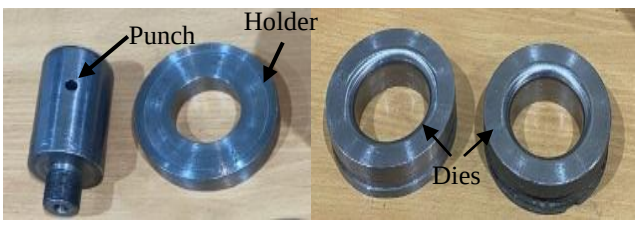

Fig. 5. Punch and dies used in this study

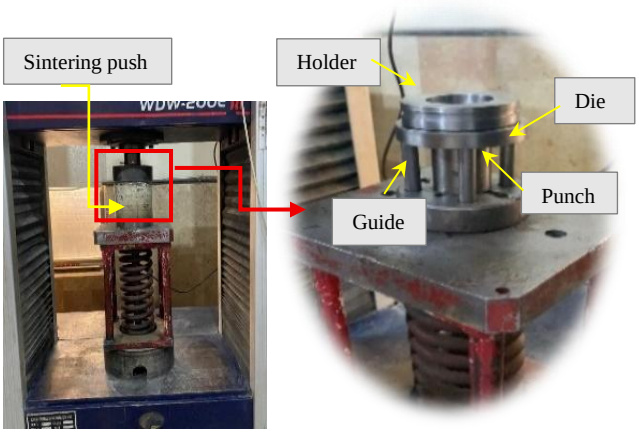

Fig. 6. Deep drawing tools

3.3. Deep drawing operation

The deep drawing experiment was conducted using a WDW200E machine 200 kN in capacity, equipped with a computerized system to record load-displacement curves. To measure their thickness after deep drawing, the cup was cut using a wire-cut, and the thickness was measured with a digital micrometer. This step was used as described in a number of research guidelines and earlier studies [19, 20]. A thorough understanding of the plastic strains can be obtained using Eq. 5 and Eq. 6 to calculate the strains in thickness ($\boldsymbol{\varepsilon}_t$), and radial directions ($\boldsymbol{\varepsilon}_r$), and Eq. 8 and Eq. 9 were used to calculate the strains in the hoop direction($\boldsymbol{\varepsilon}_\theta$), and the effective strain($\boldsymbol{\varepsilon}_{effect}$) [2, 21].

$$\varepsilon_t = \ln \frac{t}{t_0}; \quad (5)$$

$$\varepsilon_r = \ln \frac{R}{R_0}; \quad (6)$$

$$\varepsilon_\varphi = -(\varepsilon_r + \varepsilon_t); \quad (7)$$

$$\boldsymbol{\varepsilon}_{effect} = \sqrt{2/3\,(\varepsilon_r^2 + \varepsilon t^2 + \varepsilon_\varphi^2)}. \quad (8)$$

A significant consideration that determines the amount of deformation that occurs at each step of the deep drawing process is the effective incremental strain. Its value is dependent on several variables, including the blank's initial thickness (t_o) and diameter (R_o).

4. RESULTS AND DISCUSSION

In the study, a cylindrical shape was created using three different types of materials. Fig. 7 shows the punch displacements and drawing forces of these materials needed to create 1mm in thickness and 80 mm in diameter of blank to cup shapes through numerical and experimental methods. The curves demonstrate that low carbon steel requires a punch load of 47.52 kN in experimental methods and 41.2 kN for numerical methods. The reason for this high load is due to greater strength and strain hardening [5]. Brass appears after that 29.6 kN, 26.8 kN experimental and numerical, respectively. Aluminum needs the least punch load, 20.6 kN and 16 kN in both of experimental and numerical respectively, which shows that it is naturally lower strength [7]. As shown the experimentally predicted punch load is higher than the numerical values due to the simulations use it simpler material modeling and ideal

friction conditions, as also reported in studies [19, 21]. The main reasons for the slow rise in load at the start are the space between the punch and the sheet and the time it takes for the sheet to fully touch the die.

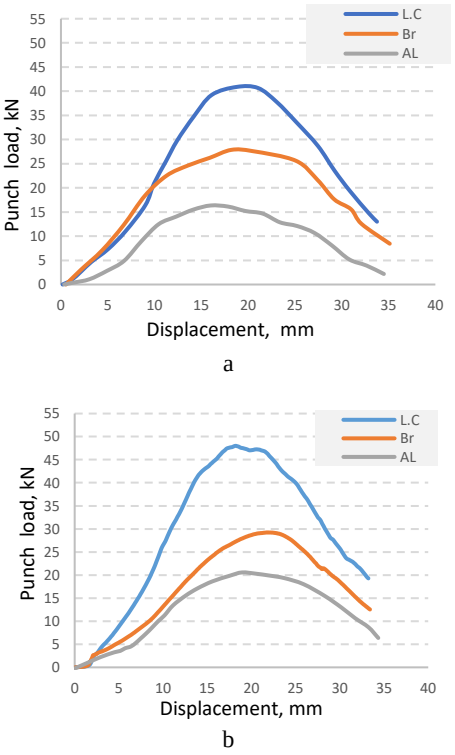

Fig. 7. Relationship between punch load and displacement in deep drawing of three different materials, at 1 mm in thickness: a – numerical; b – experimental

The results indicate that aluminum alloys offer good formability, but their performance is strongly affected by blank holder force**,** as shown in Fig. 8, the punch force-displacement curves for the experiments conducted in this study of aluminum AA1100 specimens with 80 mm in diameter and 0.7 mm in thickness of blank. Wrinkles in the flange area appear when using a low blank holder force (BHF) of 2 kN, but when using a BHF of 3 kN, the wrinkles disappear and a cup is successfully formed at a maximum punch force of 13.46 kN at 18.3 mm punch displacement. Increasing the BHF to 4 kN leads to the flange being held excessively and the tearing of the cup. The current results closely match the theoretical maximum punch force of 12.7 kN, which was reported in a prior study [22], in the same material properties in this case. Increase in sheet thickness it needs to increases in BHF. A number of variables, such as blank diameter, sheet thickness, punch and die radii, and punch speed, affect the blank holder force (BHF) for the same material, for this that result corresponds to previously released data for a cup that has a diameter of 37 mm and a sheet thickness of 0.51 mm, which required a BHF of 1.509 kN to prevent wrinkling and 2.07 kN to cause tears [23].

Fig. 9 and Fig. 10 show that for low carbon steel AISI 1008 flange wrinkling is prevented by more evenly distributed equivalent plastic stresses and strains at BHF (10 – 20 kN), and low of than this leads to local wrinkle at 8 kN and 4 kN. A blank holder force of 10 kN has been suggested by research [24, 25]. Cup of brass CuZn30 appears perfect shape at 10 kN of BHF on the other hand, excessive BHF lead to tearing of the cup.

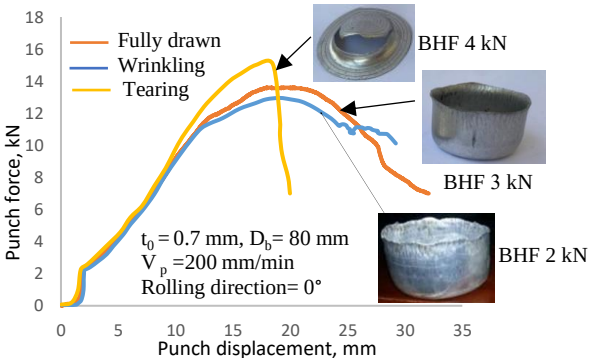

Fig. 8. Punch force-displacement curves for AL1100 blanks

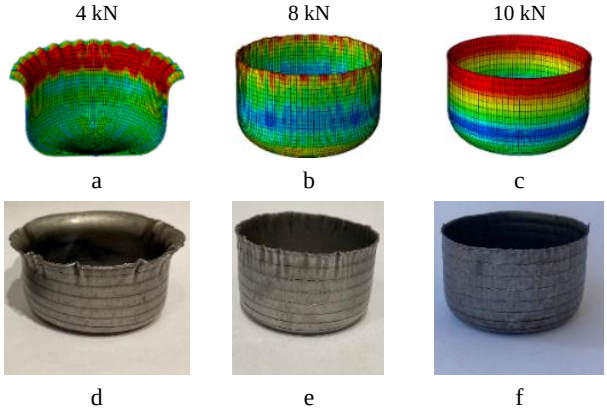

Fig. 9. Comparison of cups in simulations and experimental methods of L.C steel AISI1008, for 0.7 mm sheet thickness: a, b – the BHF is 4 kN; c, d – the BHF is 8 kN; e, f – the BHF is 10 kN

Fig. 10. Product in experimental work three types of materials in 80 mm in diameter and 0.7 in thickness: a – L.C steel AISI 1008, BHF 12 kN; b – brass CuZu30, BHF 10kN; c – aluminum AA1100, BHF 3kN

Fig. 11 and Fig. 12 show how the blank holder force affects the thickness of the cup wall.

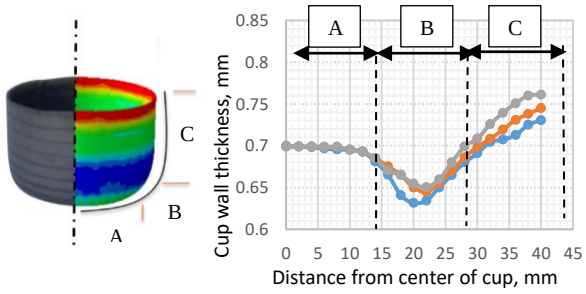

Fig. 11. The thinning zone in the final product

The figure shows that the thickness stays the same under the punch face cup bottom (A) is only partially impacted, indicating that there is not much deformation

there as a result of friction and drawing force, which are essential in reducing the possibility of distortion on the punch's flat surface. Thus, a small or no thinning occurs at region (A), then thinning increases at region (B), and more thickening becomes obvious at region (C). It is consistent with the behavior seen in the research [14, 25].

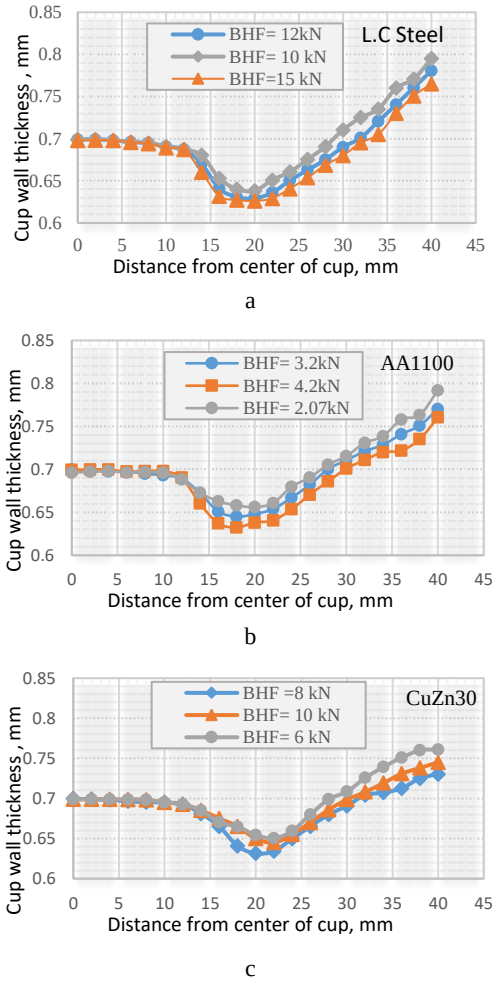

Fig. 12. Experimental effect of blank holder force variation on thickness behavior at a punch velocity of 100 mm/min and a sheet thickness 0.7 mm for: a – low carbon steel (AISI1008); b – aluminum 1100; c – brass CuZ30

The thinning will happen at the punch corner because of the stretching caused by tensile stress, and it will get worse as the blank holder force gets stronger. After that, the wall of the cup gets thicker because of the compressive stress that is put on this area. It is clear that the thickness of the cup wall gets thinner as the blank holder force gets stronger. It is observed that the optimal thickness distribution across all zones in the produced cup is achieved when employing a blank holder force of 12 kN. Fig. 13 – Fig. 21 and Table 5 illustrate the effect of various forming parameters on thickness distribution for all three metals, low carbon steel (AISI 1008 L.C steel), aluminum (AA1100), and brass (CuZn30) in both experimental (EXP) and finite element simulation (FES). It was found that lower blank sheet thickness and lower punch speed led to less thinning for low carbon steel AISI 1008 and brass CuZn30, that is due to strain localization. The minimum thinning was seen along the 90° and the maximum thinning at 45° in rolling direction, these patterns are associated with Lankford anisotropy as shown in Table 4, in which higher *r*-values decrease thinning, while lower *r*-values increase thinning. However, for AA1100 it seen that at 45° direction has the lower thinning values under certain forming conditions, indicating that thinning behavior doesn't always affect by plastic anisotropy. Previous investigations have shown that is also influenced by strain rate sensitivity, material softness, and frictional effects in addition to plastic anisotropy [7, 8]. Regions (B) at punch noise show the most thinning at the highest punch speed of 200 mm/min, higher punch speed in AA1100 led to rapid material deformation, which reduces the time available for proper redistribution of the blank [26]. While the least thinning is more stable and uniform at the lower speed of 100 mm/min for the three materials. This result aligns with the behavior of the conical product of low carbon steel and galvanized material found in the research [18, 25]. When the die corner radius (*R*) decreases, thinning increases, and a smaller (*R*) increases strain concentration and causes more wall thinning [11].

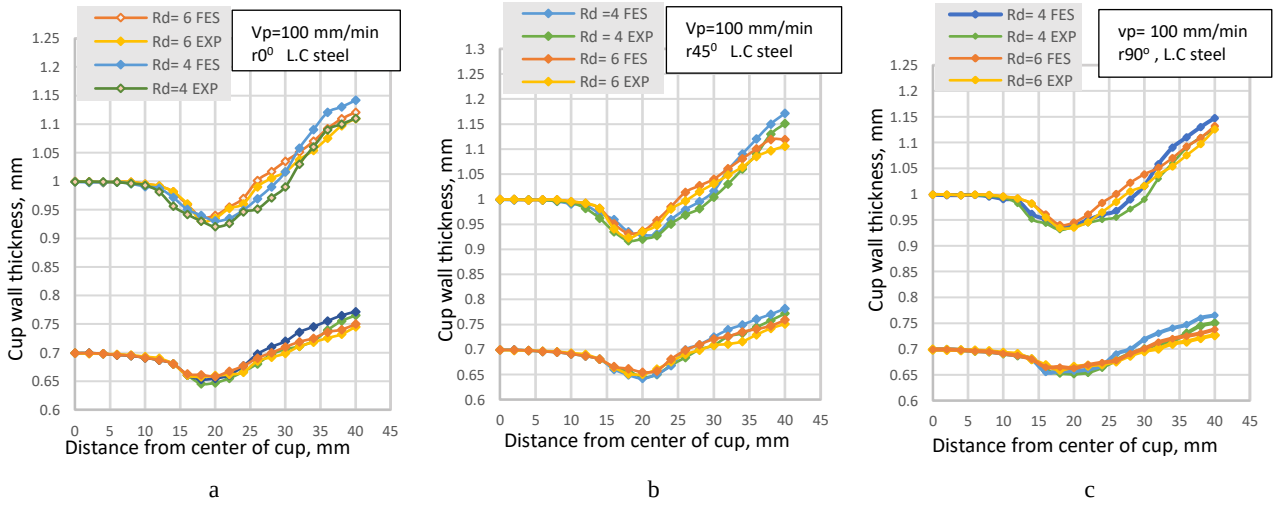

Fig. 13. Effect of die radius variation on thickness behavior of L.C steel AISI with sheet thickness of 0.7 and 1 mm at punch velocity 100 mm/min along: a – 0° rolling direction; b – 45° diagonal direction; c – 90° transverse direction, experimental and numerical

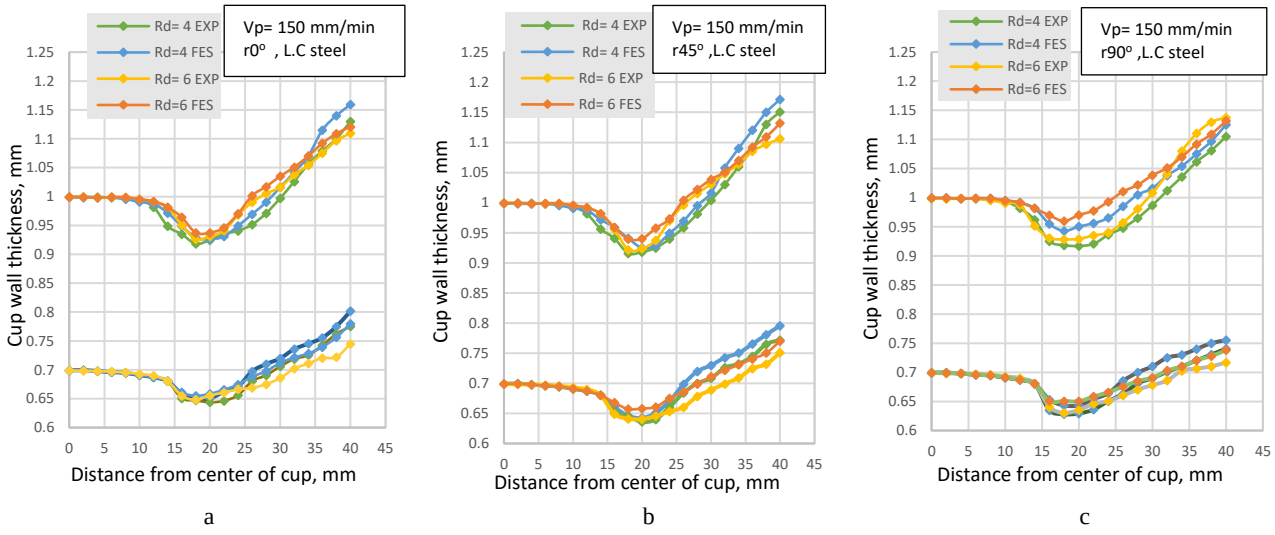

a b c

Fig. 14. Effect of die radius variation on thickness behavior of L.C steel AISI with sheet thickness of 0.7 and 1 mm at punch velocity 150 mm/min along: a – 0° rolling direction; b – 45° diagonal direction; c – 90° transverse directions, experimental and numerical

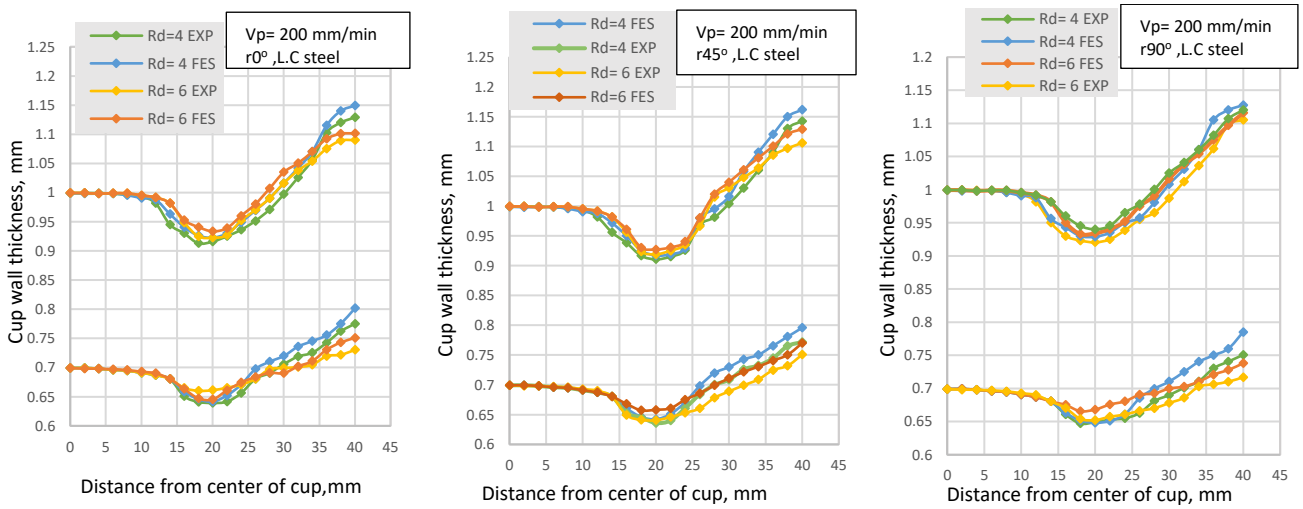

a b c

Fig. 15. Effect of die radius variation on thickness behavior of L.C steel with sheet thickness of 0.7 and 1 mm at punch velocity 200 mm/min along: a – 0° rolling direction; b – 45° diagonal direction; c – 90° transverse directions, experimental and numerical

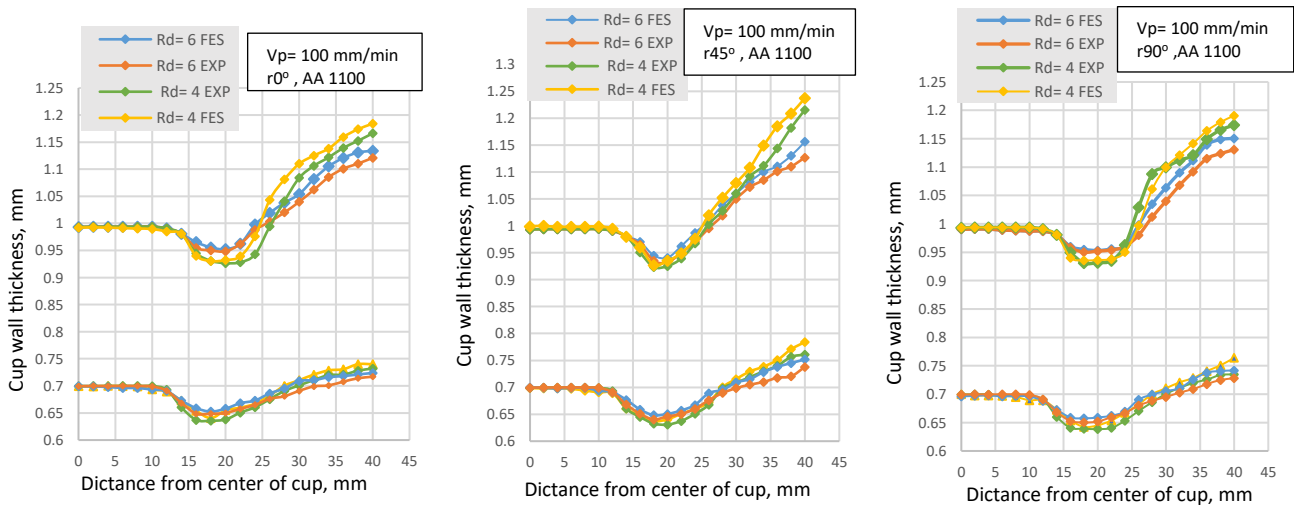

a b c

Fig. 16. Effect of die radius variation on thickness behavior of aluminum 1100 with sheet thickness of 0.7 and 1 mm at punch velocity 100 mm/min along: a – 0° rolling direction; b – 45° diagonal direction; c – 90° transverse directions, experimental and numerical

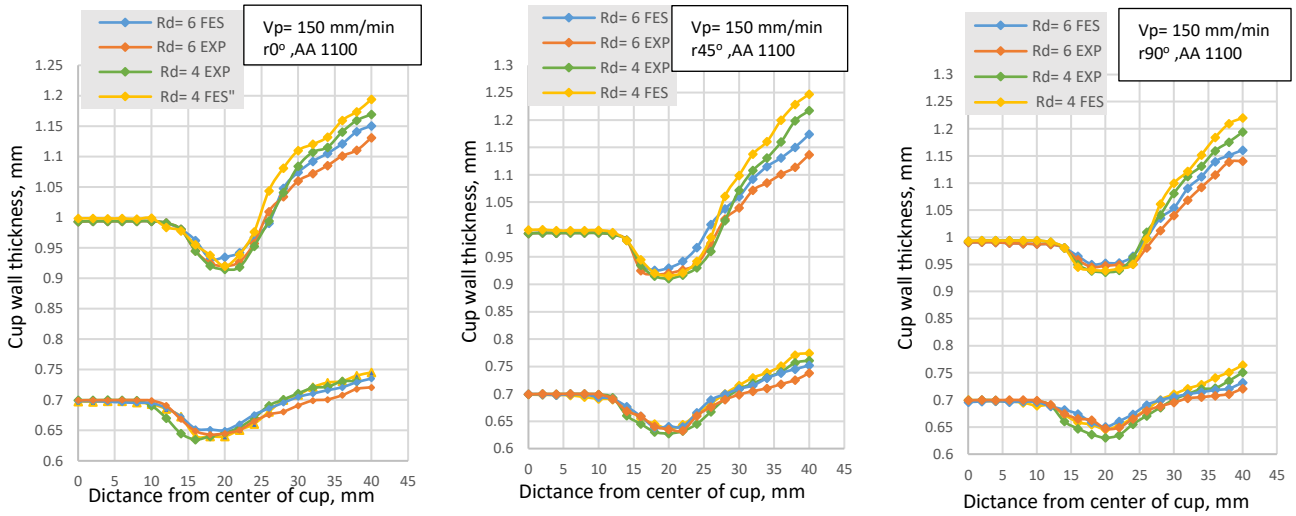

a b c

Fig. 17. Effect of die radius variation on thickness behavior of aluminum 1100 with sheet thickness of 0.7 and 1 mm at punch velocity 150 mm/min along: a – 0° rolling direction; b – 45° diagonal direction; c – 90° transverse directions, experimental and numerical

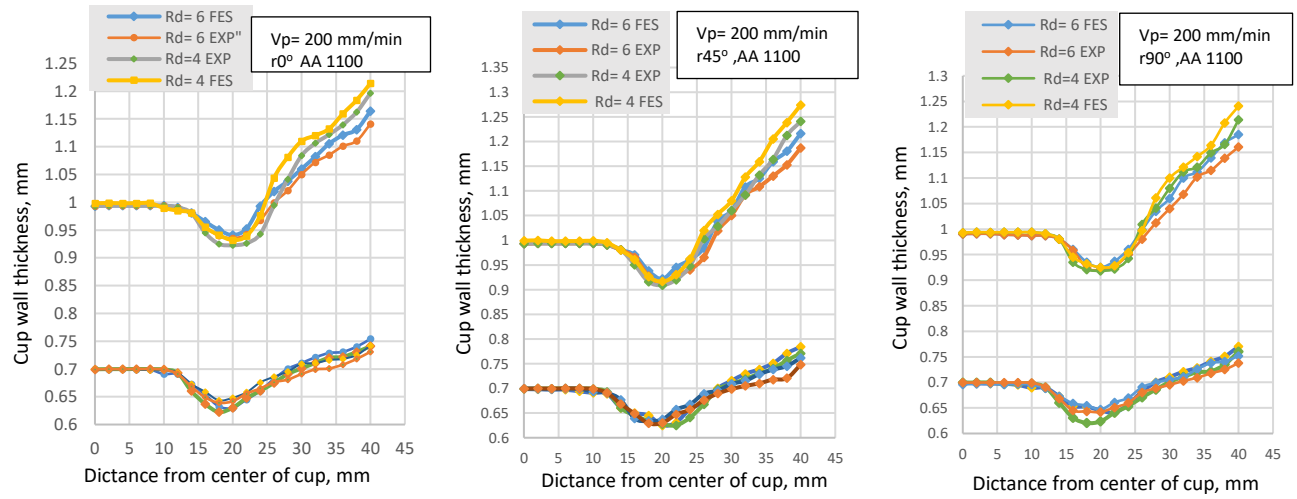

a b c

Fig. 18. Eeffect of die radius variation on thickness behavior of aluminum 1100 with sheet thickness of 0.7 and 1 mm at punch velocity 200 mm/min along: a – 0° rolling direction; b – 45° diagonal direction; c – 90° transverse directions, experimental and numerical

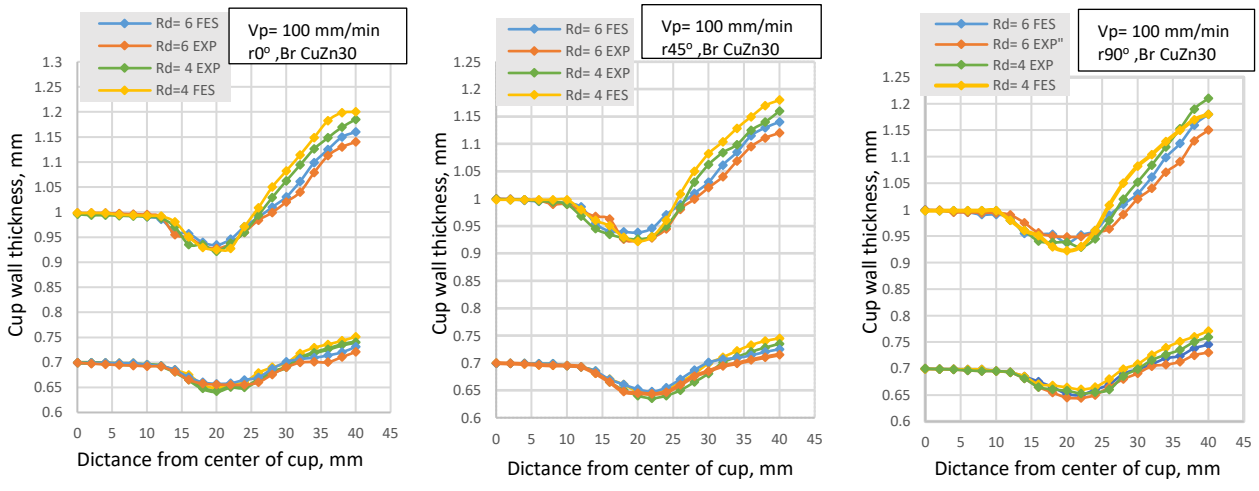

a b c

Fig. 19. Eeffect of die radius variation on thickness behavior of brass CuZn30 with sheet thickness of 0.7 and 1 mm at punch velocity 100 mm/min along: a – 0° rolling direction; b – 45° diagonal direction; c – 90° transverse directions, experimental and numerical

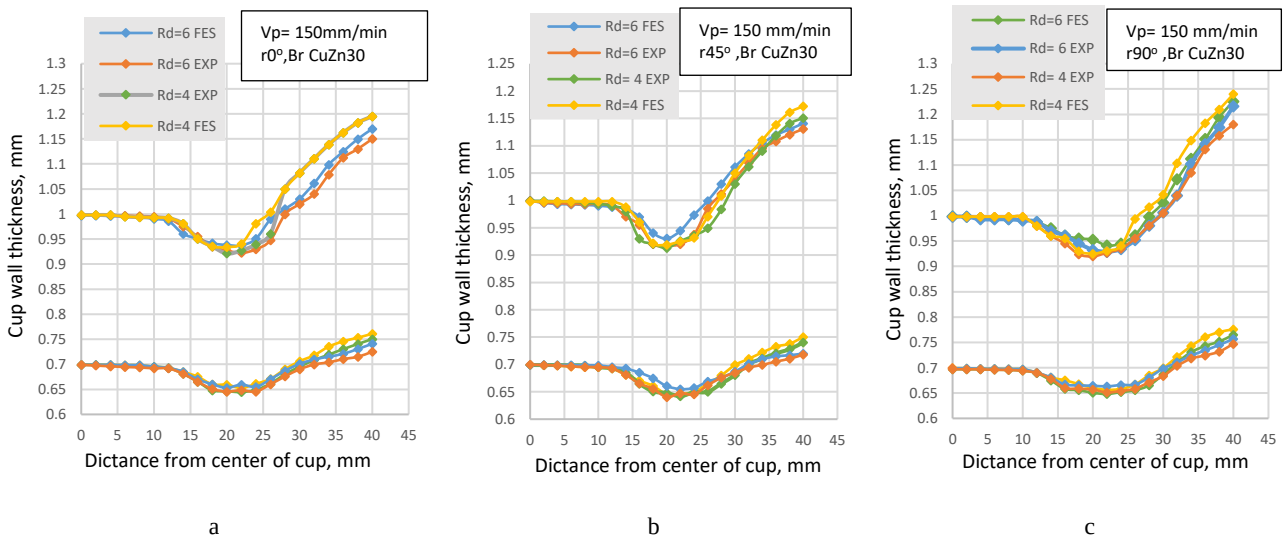

a b c

Fig. 20. Eeffect of die radius variation on thickness behavior of brassCuZn30 with sheet thickness of 0.7 and 1 mm at punch velocity 150 mm/min along: a – 0° rolling direction; b – 45° diagonal direction; c – 90° transverse directions, experimental and numerical

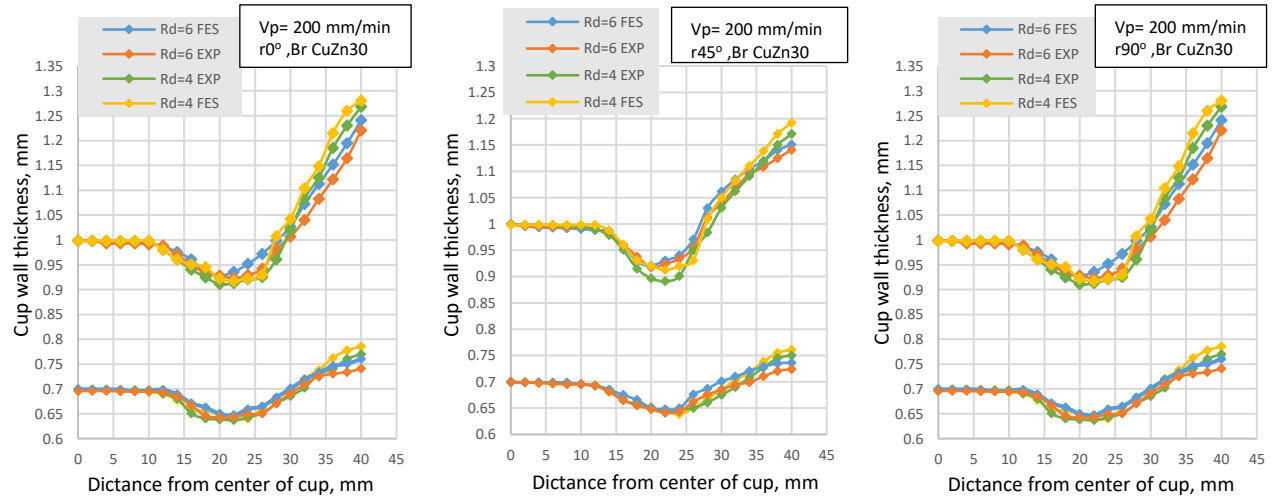

a b c

Fig. 21. Eeffect of die radius variation on thickness behavior of brassCuZn30 with sheet thickness of 0.7 and 1 mm at punch velocity 200 mm/min along: a – 0° rolling direction; b – 45° diagonal direction; c – 90° transverse directions, experimental and numerical

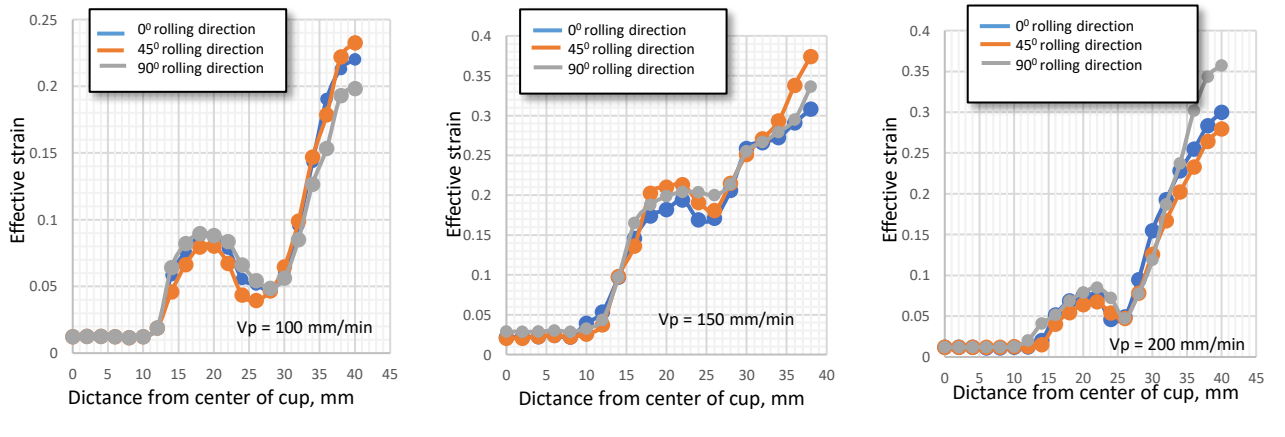

a b c

Fig. 22. The variations of effective strain of L.C Steel with blank sheet 1 mm at varying punch velocity for: a – simulation FES; b – experimental work EXP

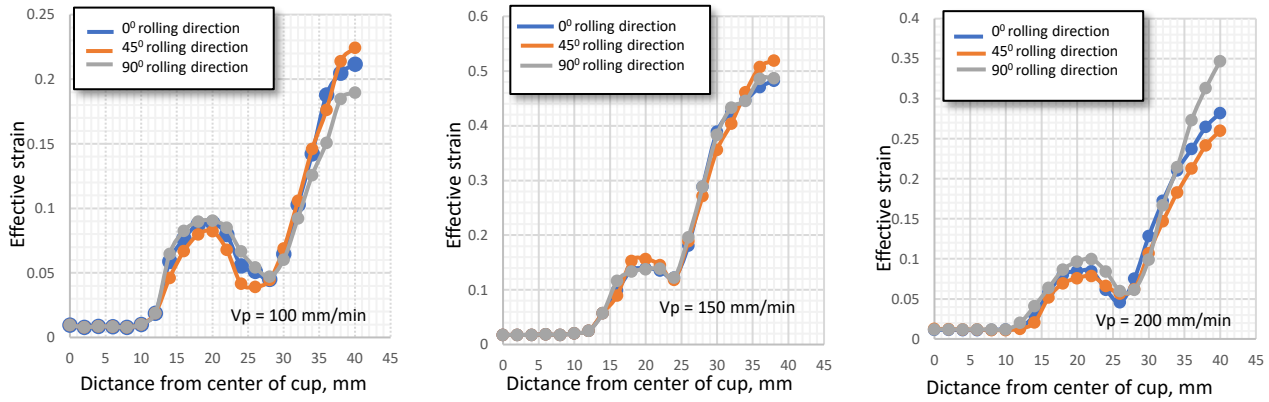

a b c

Fig. 23. The variations of effective strain of L.C Steel with blank sheet 1mm at varying punch velocity for: a – simulation FES; b – experimental work EXP

Table 5. % Thinning values

Material type	Sheet thickness, mm	Die radius	Angle from the rolling direction, °	% Thinning – EXP			% Thinning – FES		
				Punch velocity, mm/min			Punch velocity, mm/min		
				100	150	200	100	150	200
Low carbon steel AISI 1008	0.7	6	0	6.06	7.40	7.55	5.56	6.42	6.70
			45	6.93	7.79	8.41	6.45	7.28	7.76
			90	5.69	5.81	6.70	4.98	6.71	6.83
		4	0	7.53	8.02	9.57	6.69	7.18	7.26
			45	8.00	8.53	8.76	7.16	7.85	8.38
			90	6.74	6.80	11.27	6.18	6.71	7.04
	1	6	0	7.00	7.40	7.80	6.27	6.40	6.64
			45	7.70	7.90	8.10	6.80	7.07	7.28
			90	6.51	6.66	6.80	5.95	6.27	6.98
		4	0	7.96	8.17	8.70	6.96	7.38	7.73
			45	8.27	8.42	8.94	7.17	7.50	8.29
			90	6.92	7.30	7.95	6.37	6.70	7.10
Aluminum 1100	0.7	6	0	7.27	7.85	7.67	6.36	7.00	7.07
			45	7.73	9.24	10.39	7.10	8.49	9.48
			90	7.10	7.30	8.28	5.93	6.38	7.53
		4	0	8.02	9.26	10.13	7.35	8.56	9.25
			45	8.49	9.93	12.42	8.07	9.13	10.00
			90	7.76	8.53	12.33	7.39	7.84	9.15
	1	6	0	7.18	7.28	7.29	6.26	6.91	7.70
			45	7.66	8.99	8.76	7.08	7.43	7.83
			90	6.47	7.27	7.98	5.06	6.13	7.46
		4	0	7.93	8.54	8.93	7.49	8.01	8.23
			45	8.24	8.94	9.0	7.59	8.41	8.35
			90	7.49	7.94	8.15	7.19	7.53	7.46
Brass CuZu30	0.7	6	0	6.38	7.38	8.24	5.99	6.71	7.09
			45	6.65	7.52	8.10	6.09	7.66	7.42
			90	6.13	6.95	7.40	5.87	6.21	6.69
		4	0	7.14	7.92	8.10	6.22	7.02	7.50
			45	7.78	8.12	8.34	7.08	7.67	8.20
			90	6.31	7.40	7.93	6.22	6.22	6.89
	1	6	0	7.25	7.77	8.09	6.58	7.89	8.48
			45	7.68	8.24	8.26	7.18	8.29	8.90
			90	6.85	7.10	7.70	6.28	7.11	7.20
		4	0	8.01	9.88	11.21	7.88	8.89	9.48
			45	8.30	10.71	12.31	8.10	9.78	11.75
			90	7.06	9.01	10.91	7.48	8.78	9.28

Excessive thinning above 20 % of the initial thickness is considered an unacceptable part. The thinning percentage is determined from [2, 18, 19]:

$$\% \text{ thinning} = \frac{t_0 - t}{t_0} \times 100\ \%. \quad (9)$$

Fig. 22, and Fig.23 show the forming technique used in deep drawing processes and how it affects the distribution of equivalent strains throughout the cup wall. Manufacturers can create cups with the required final shape and mechanical qualities by improving the forming process.

4. CONCLUSIONS

1. The finite element results using ABAQUS showed an excellent agreement with the experimental findings, with a maximum discrepancy of about 5 %.
2. The blank holder force must be maintained within an optimal range to avoid defects. Low BHF values (< 10 kN for AISI 1008 and CuZn30) cause wrinkling, whereas excessive BHF leads to tearing, particularly in aluminum 1100 near punch corners. In addition, thinning increases near the punch nose as the blank holder force increases, while thickening develops near the flange region. Therefore, selecting the right BHF is essential to achieve an even thickness and avoid tearing and wrinkling failure.
3. Increasing the sheet thickness for AISI1008 and CuZn30 results in greater thinning. This occurs because thicker blanks, are held more tightly by the blank holder, leading to enhanced local deformation and strain, while thinning increases with decreasing sheet thickness for AA1100 under the investigated forming conditions. This result confirms that thinning is affected by strain-rate sensitivity, high material softness, and adhesion-related friction. Low carbon steel (AISI 1008) demonstrated higher strength and resistance to thinning, while brass CuZn30 exhibited intermediate performance with uniform deformation under suitable conditions.
4. Increasing the forming (punch) speed and reducing the die corner radius (R) led to an increase in thinning and strain concentration for the three materials. The best thickness distribution for all zones in the produced cup was achieved with a punch velocity of 100 mm/min and a die corner radius of 6 mm.
5. The values of Lankford coefficients affect the thinning behavior. where higher r-values usually reduce thinning. AISI 1008 steel and CuZn30 brass indicated minimum thinning along the 90° transverse direction. whereas AA1100 aluminum had a more complicated strain response. The highest thinning appears at the 45° rolling direction because of factors beyond plastic anisotropy.

Acknowledgments

The author gratefully acknowledges the Production and Metallurgy Engineering Department, University of Technology-Baghdad, for providing access to the necessary equipment and laboratories used in this study.

REFERENCES

1. **Pradipkumar, N.P., Inamdar, K.H.** A Review on Deep Drawing of Rectangular Shaped Part *Asian Journal of Convergence in Technology.* 2 2016: pp. 1 – 3.
2. **Hosford, K.B.W.F., Caddell, R.M.** Metal Forming: Mechanics and Metallurgy, *3rd edition. Cambridge, MA, USA: Cambridge University Press*, 2007.
3. **Mohammed, A.I.** Analysis of Forming Complex Cup by Drawing Process *IOP Conference Series Material Since and Engineering*. 881 2020: pp. 012055. https://doi.org/10.1088/1757-899X/881/1/012055
4. **Reddy, P.V.R.R., Rao, B.V.S., Reddy, G.C.M., Prasad, P.R.** Parametric Studies on Wrinkling and Fracture Limits in Deep Drawing of Cylindrical Cup *International Journal of Emerging Technology and Advanced Engineering* 2 (6) 2012: pp. 218 – 222.
5. **Khelifi, S., Ayad, A., Boumaiza, A., Rouag, N., Wagner, F., Ji, V.** Correlations Between XRD Peak Broadening and Elastic and Plastic Deformation for Mild Steel Sheets Under Tensile Loading *Materials Science (Medžiagotyra*) 30 (3) 2024: pp. 414 – 422. https://doi.org/10.5755/j02.ms.36098
6. **Skakun, P., Rajnovic, D., Janjatovic, P., Movrin, D., Dramicanin, M., Berus, L., Ficko, M.** Experimental Determination of a Strain State in a Bulk Forming of a Low Carbon Steel *Materials Science (Medžiagotyra)* 30 (1) 2024: pp. 40 – 46. http://doi.org/10.5755/j02.ms.34605
7. **Rajhi, W.** Numerical Simulation of Damage on Warm Deep Drawing of Al 6061-T6 Aluminium Alloy *Engineering Technology & Applied Science Research* 9 (5) 2019: pp. 4830 – 4834. https://doi.org/10.48084/etasr.3148
8. **Ha, J., Fones, J., Kinsey, B.L., Korkolis, Y.P.** Plasticity and Formability of Annealed, Commercially-Pure Aluminum Experiments and Modeling *Materials* 13 (19) 2020: pp. 4285. https://doi.org/10.3390/ma13194285
9. **Luštinec, J., Roško, M., Očenášek, V.** Structural and Mechanical Properties of CuZn30 Cartridge Brass in Real Production Conditions *Manufacturing Technology* 23 (6) 2023: pp. 846 – 852. https://doi.org/10.21062/mft.2023.090
10. **Ganjiani, M., Ghobadi, S., Faraji, G.** Evaluating the Ductile Failure Characteristics of CuZn30 Brass under Different Stress Conditions *Engineering Failure Analysis* 167 2025: pp. 108932. https://doi.org/10.1016/j.engfailanal.2024.108932
11. **El Sherbiny, M., Zein, H., Abd-Rabou, M.** Thinning and Residual Stresses of Sheet Metal in the Deep Drawing Process Materials & *Design* 55 2014: pp. 869 – 879. http://doi.org/10.1016/j.matdes.2013.10.055
12. **Bouchaâla, K., Ghanameh, M.F., Faqir, M.** Numerical Investigation of the Effect of Punch Corner Radius and Die Shoulder Radius on the Flange Earrings for AA1050 and AA1100 Aluminum Alloys in Cylindrical Deep Drawing Process *Heliyon* 7 (4) 2021. pp. e06662. https://doi.org/10.1016/j.heliyon.2021.e06662
13. **Zein, H., El Sherbiny, M., Abd-Rabou, M.** Thinning and Springback Prediction of Sheet Metal in the Deep Drawing Process *Materials & Design* 64 2014: pp. 797 – 808. https://doi.org/10.1016/j.matdes.2013.10.055
14. **Tomáš, M., Evin, E., Kepič, J., Hudák, J.** Physical Modelling and Numerical Simulation of the Deep Drawing Process of a Box-Shaped Product Focused on Material Limits Determination *Metals* 9 (10) 2019: pp. 1058. https://doi.org/10.3390/met9101058
15. **Mousa, A.A.A., Khalifa, A.A., Jweeg, M.J.** Numerical and Experimental Studies of the Formability of the Low Carbon Steel (AISI 1008) by Using Hydromechanical Deep Drawing *Materials Today: Proceedings* 60 2022: pp. 1721 – 1730. https://doi.org/10.1016/j.matpr.2021.12.305
16. **Choubey, A.K., Sasikumar, C.** Effect of Anisotropy, Temperature, and Strain Rate on Deep Drawing Using

Conical Die *Journal of Metallic Material Research* 3 (1) 2020: pp. 20 – 24. https://doi.org/10.30564/jmmr.v3i1.920

17. **Chen, K., Carter, A.J., Korkolis, Y.P.** Earing Reduction by Varying Blank Holding Force in Deep Drawing of Aluminum Alloy Sheets *Metals* 11 (3) 2021: pp. 395. https://doi.org/10.3390/met11030395
18. **Jweeg, M.J., Mohammed, A.I., Jabbar, M.S.** Investigation of Thickness Distribution Variation in Deep Drawing of Conical Steel Products *Engineering and Technology Journal* 39 (4A) 2021: pp. 586 – 598. https://doi.org/10.30684/etj.v39i4A.1908
19. **Mohsein, Z.H., Hameed, A., Abass, W.** Experimental and Analytical Investigation of the Deep Drawing Process for Producing Pentacle Cups *Engineering, Technology & Applied Science Research* 14 (3) 2024: pp. 13856 – 13863. https://doi.org/10.48084/etasr.7074
20. **Arjunan, V., Pasupathy, G.** Multi Objective Optimisation of Metal Die Support Incremental Sheet Forming of SS 316L Sheets Using Taguchi Grey Relational Analysis *Materials Science (Medžiagotyra)* 31 (2) 2025: pp. 162 – 170. https://doi.org/10.5755/j02.ms.38056
21. **Jawad, W., Ikal, A**. Effect of Radial Clearance on Stress and Strain Distribution in the Astral Deep Drawing *Engineering and Technology Journal* 37 (8A) 2019: pp. 332 – 340. https://doi.org/10.30684/etj.37.8A.4
22. **Hussein, N.Z., Ameen, H.A., Saleh, A.H.** Effect of the Location of Draw Bead and Its Profile in Cylindrical Cup Forming *IOP Conference Series: Materials Science and Engineerin*g 881 2020: pp. 012054. https://doi.org/10.1088/1757-899X/881/1/012054
23. **Chen, K.A., Carter, A.J., Korkolis, Y.P.** Flange Wrinkling in Deep-Drawing: Experiments, Simulations, and Reduced-Order Model *Journal of Manufacturing and Materials Processing* 6 2022: pp. 27. https://doi.org/10.3390/jmmp6040076
24. **A Demirci, H.I., Esner, C., Yasar, M.** Effect of the Blank Holder Force on Drawing of Aluminum Alloy Square Cup: Theoretical and Experimental Investigation *Journal of Materials Processing Technology* 206 2008: pp. 152 – 160. https://doi.org/10.1016/j.jmatprotec.2007.12.010
25. **Abdullah, M.A., Abed, A.H., Mansor, K.K.** Comparison Between Low-Carbon Steel and Galvanized Steel by Deep Drawing Under the Influence of Different Parameters *Materials Performance and Engineering* 33 (2) 2025: pp. 163 – 170. https://doi.org/10.2478/mspe-2025-0016
26. **Hedayati, E., Hedayati, A., Vahedi, M., Faroughi, S.** Numerical Investigation of the Impact of Punch Speed on the Deep Drawing of Square Aluminum Sheet Using Finite Element Method *American Journal of Engineering and Applied Sciences* 18 (1) 2025: pp. 39 – 46. https://doi.org/10.3844/ajeassp.2025.39.46